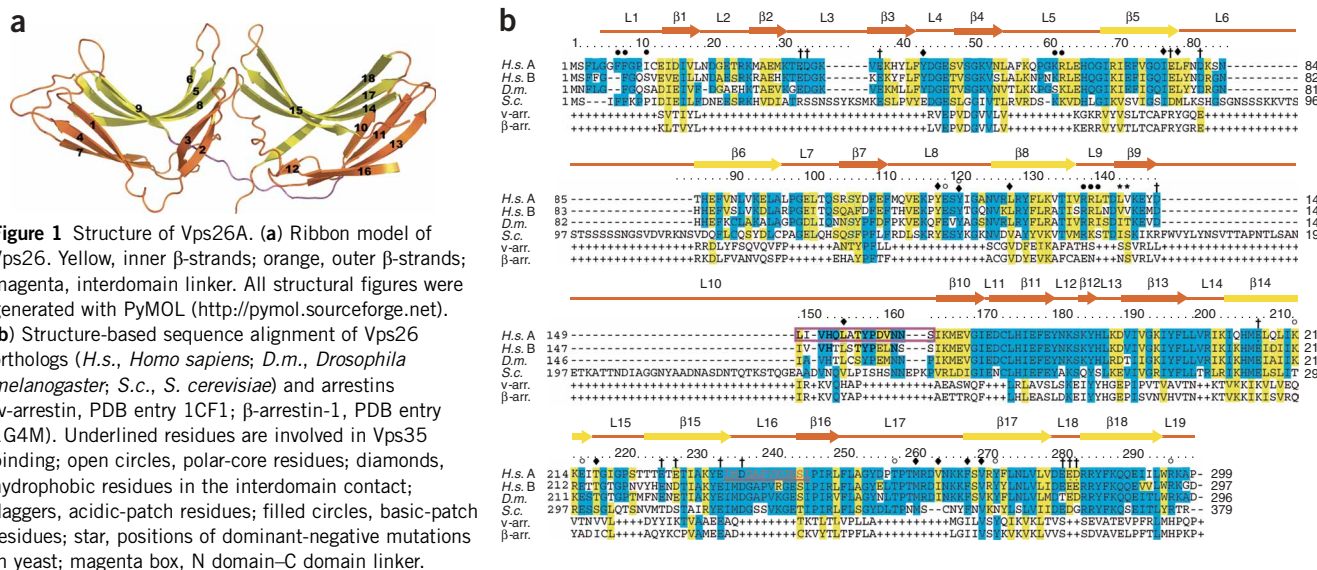


Hang Shi^{1,3,4}, Raul Rojas^{2,4}, Juan S Bonifacino² & James H Hurley¹

The function of the Vps26 subunit has been the least clear of any of the five subunits. There are no homologous proteins of known structure or function and few clues as to its role within the complex. Vps26 is required for embryonic development in mice²⁵ and is downregulated in Alzheimer disease²⁶, highlighting its importance in mammalian physiology. Two isoforms of Vps26, Vps26A and Vps26B,

Received 8 December 2005; accepted 3 May 2006; published online 28 May 2006; doi:10.1038/nsmb1103



are encoded by the mouse genome, and both can interact with other retromer subunits²⁷. To further understand the assembly of the retromer and the function of Vps26 in retrograde trafficking, we solved the structure of human Vps26A (herein referred to as Vps26) at 2.1-Å by X-ray crystallography. The structure reveals that Vps26 is a close structural relative of the arrestins, an extensively characterized family of proteins involved in receptor internalization at the plasma membrane²⁸. Vps26 shares not only the same overall fold as the arrestins, but an unusual polar core as well. Using a combination of structure-based mutagenesis and yeast two-hybrid assays, we show that Vps26 interacts directly with Vps35 through a loop near the distal tip of the C-terminal domain. This interaction is essential for the assembly of Vps26 into the retromer complex and its recruitment to endosomes in mammalian cells, and for function of the retromer complex in vacuolar sorting of CPY in yeast. The combination of structural homology, the known properties of the arrestins and the mapping of the Vps35-binding site onto the structure allows us to advance a working model for the function of this subunit.

RESULTS

Structure determination of Vps26

The full-length 327-residue human Vps26 protein crystallizes in space group $P2_12_12_1$. The crystal structure was determined using MAD from both selenomethionine (SeMet)-substituted protein crystals and platinum-soaked derivative crystals, together with isomorphous replacement using native and platinum-derivative crystals (Supplementary Fig. 1 online). Vps26 behaves as a monomer in solution during purification and packs as one molecule per asymmetric unit in the crystal. Within the crystal, tubes that run the length of the crystal are formed where concavities in each Vps26 monomer are juxtaposed to each other (Supplementary Fig. 2 online). The refined model contains residues 6–299 with a gap between 239 and 244 owing to missing electron density. Residue 161 on

the linker between two domains also shows poor density. The final model was refined to 2.1 Å with $R_{\text{free}} = 28\%$ and $R\text{-factor} = 23\%$.

Molecular architecture of Vps26

The Vps26 molecule consists of two domains; each of them folds into a deeply curved β -sandwich (Fig. 1a). Each sandwich is formed by a four-stranded antiparallel β -sheet packed against an antiparallel β -sheet of three or four strands in the N-terminal domain (N domain) or C-terminal domain (C domain), respectively. The N domain contains residues 6–148 and the C domain includes residues 164–299. There is a 15-residue loop, from 149 to 163 (L10), that connects the two domains. This loop is relatively mobile, with poor electron density for several residues centered on Asn161. The N domain and the C domain are related by an intramolecular pseudo two-fold rotation axis, and their superposition using 59 C α atoms from core β -strands yields an r.m.s. deviation of 1.5 Å. The surface of the inner β -sheet of each domain is polar. Residues at the outer layer of the β -sandwich from the C domain have high B -factors (above 70 Å² on average), with residues 239–244 missing from the electron density map, indicating that this region is more mobile than the rest of the protein.

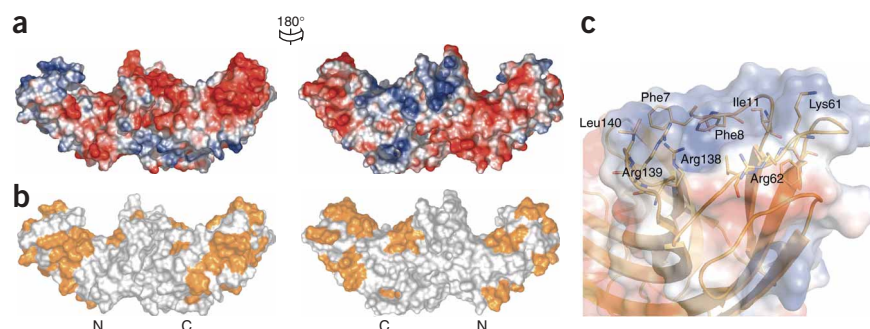


Figure 2 Surface properties of Vps26. (a) Electrostatic potential. Surfaces are colored with saturating blue and red at ± 5 kT e⁻¹. (b) Residues altered in site-directed mutagenesis (Table 1) are colored in orange. (c) Potential membrane-binding site shown in surface representation and colored with saturating blue and red at ± 5 kT e⁻¹. Hydrophobic residues and positively charged residues are shown in orange ball-and-stick representation.

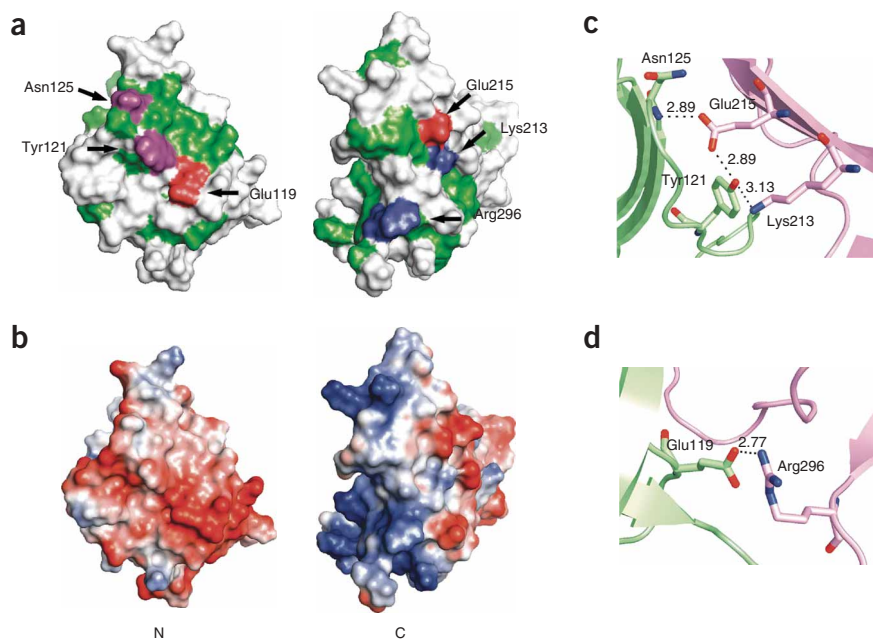


Figure 3 Polar core of Vps26. (a) Polarity of interface between the two domains. Green, hydrophobic residues; white, polar residues; red, acidic residues buried in the polar core; magenta, uncharged residues involved in hydrogen bonding; blue, basic residues. (b) Electrostatic potential at the interface is colored with saturating blue and red at $\pm 5 \text{ kT e}^{-1}$. (c,d) Residues contributing to the first (c) and second (d) clusters of polar interactions are shown in ball-and-stick representation. Hydrogen bond distances (Å) are indicated. Green, N domain; pink, C domain.

The interface between the N domain and the C domain buries $1,964 \text{ Å}^2$ of solvent-accessible surface area (Fig. 3), including 700 Å^2 of polar surface and $1,264 \text{ Å}^2$ of nonpolar surface. The hydrophobic interaction is formed by residues from the body of the N domain, the body of the C domain and the linker loop. Twelve hydrophobic residues participate in this interaction. An extensive buried polar core is formed between the two domains (Fig. 3a,b). The polar core includes N domain residues Glu119 and Tyr121 and

C domain residues Lys213, Glu215, Thr258, Tyr272 and Arg296 (Figs. 1 and 3). The most extensive buried hydrogen bond network occurs between the Tyr121, Lys213 and Glu215 side chains and the main chain amino groups from Ala124 and Asn125 (Fig. 3c). The second network is formed by a buried salt bridge between Glu119 and Arg296 (Fig. 3d). With the exception of Lys213, residues involved in forming these interactions are highly conserved in Vps26 proteins, suggesting that they are crucial in protein function (Fig. 1b).

Structural homology to the arrestins

The fold of Vps26 closely resembles that of the arrestin family members, despite the absence of detectable sequence similarity (Fig. 4), as shown by a search of the Protein Data Bank³⁰. Superimposing Vps26 with visual arrestin (v-arrestin)³¹ using C α s of corresponding β -strands results in r.m.s. deviations of 1.4 Å between N domains (63 C α atoms) and 1.5 Å between C domains (94 C α atoms). One of the defining features of arrestin family proteins is the existence of a polar core embedded between the two domains. Vps26 shares this feature in the general sense that the domain interface

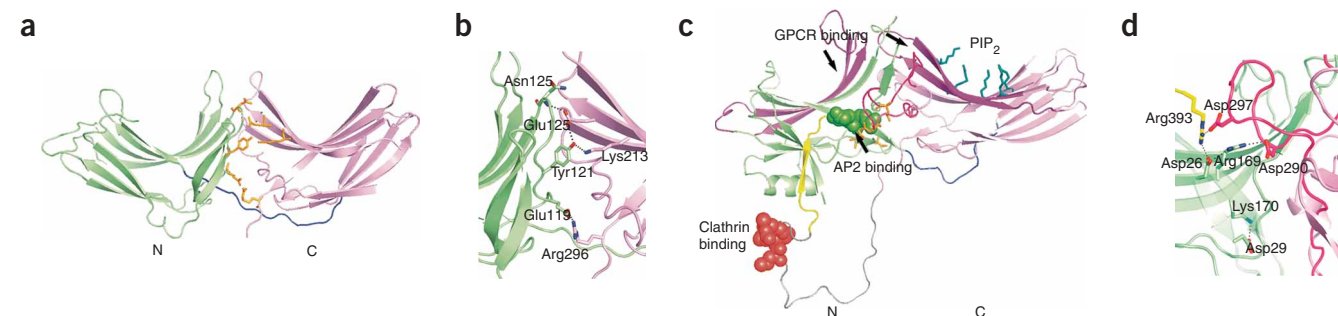


Figure 4 Structural similarities between Vps26 and β -arrestin. (a) Vps26 shown as a ribbon. Green, N domain; pink, C domain; blue, interdomain linker; orange, polar-core residues. (b) Polar-core residues in Vps26. (c) β -arrestin-1 shown as a ribbon, colored as in a. Gray, disordered region at the C tail, modeled in an arbitrary conformation; red spheres, clathrin-binding site; green spheres, AP-2-binding site; purple, GPCR-binding sites in the N and C domain cups; turquoise ball-and-stick side chains, PIP₂-binding residues; magenta, C domain lariat; yellow, C-terminal tail. (d) Polar-core residues in β -arrestin-1.

Table 1 Summary of Vps26 mutant phenotypes

Mutant number	Mutations ^a	Vps35 binding in two-hybrid assay ^b	Assembly with Vps35, Vps29 <i>in vivo</i> ^c	Endosomal localization in cells ^d	Rescue of CPY processing in <i>vps26Δ</i> yeast ^e	Rescue of CPY secretion in <i>vps26Δ</i> yeast ^e
–	WT	++	+	+	+	+
1	L431A V144D K145D	++				
2	E13A D15A	++				
3	K133D T135D V137D	++				
4	R69A E71A	++	+	+		
5	L97D	++				
6	R127E R129E F131E	++				
7	F79D	++				
8	R271E F273E	++				
9	K214E I216E	++				
10	T225D T227D	++				
11	I230D Y233D	++				
12	L250D F251D	++				
13	F197D L198D	++				
14	V200D I204D	++				
15	I246D	++				
16	I235D M236D / I318D M319D	–	–	–	–	–
17	R284E R285E F287E	++				
18	Δ238–246 GG / Δ321–328 GG	–	–	–	–	–
19	V190D V192D K194D	++				
20	E177A E179A K182D	++				
21	E165D K167A	++				
22	E171A D172A	++				
23	E281A E182A D183A R284A	++				
24	S49A K51D N53A	++				
25	V137D R139D L140D	++				
26	T102D Q103D R105D	++				
27	D108A E110A M112D	++				
28	V53A A55D K57D	++				
29	K61A R62D E64D	++				
30	E234A D237A	++				
31	I235D	+				
32	M236D	+				
33	G238P / G321P	±	–	–	–	–
34	238–246 polyS / 321–328 polyS	±	–	–	–	–
35	Y121F / Y150F			+		+
36	N125R / N155D			+		+
37	E215R / E298R			+		+
38	R296E / R377E			+		+

^aFor mutations made in both human and yeast proteins, slash separates human position / equivalent yeast position. ^bYeast two-hybrid assays were performed as in **Figure 5**. ++, normal growth; +, reduced growth in the presence of 10 mM 3-AT; ±, lack of growth in the presence of 10 mM 3-AT; –, no growth. ^cCoprecipitation of Vps35 and Vps29 with wild-type or mutant Vps26-myc expressed by transfection in HeLa cells was performed as in **Figure 6**. +, normal assembly; –, reduced or no assembly. ^dColocalization (+) or lack thereof (–) of wild-type or mutant Vps26-myc with SNX1 on endosomes in HeLa cells, analyzed as in **Figure 6**. For each condition, 50–75 cells from three independent experiments were examined. ^eCPY processing and secretion were analyzed as in **Figure 7**. For both assays, + denotes normal function and – denotes reduced function.

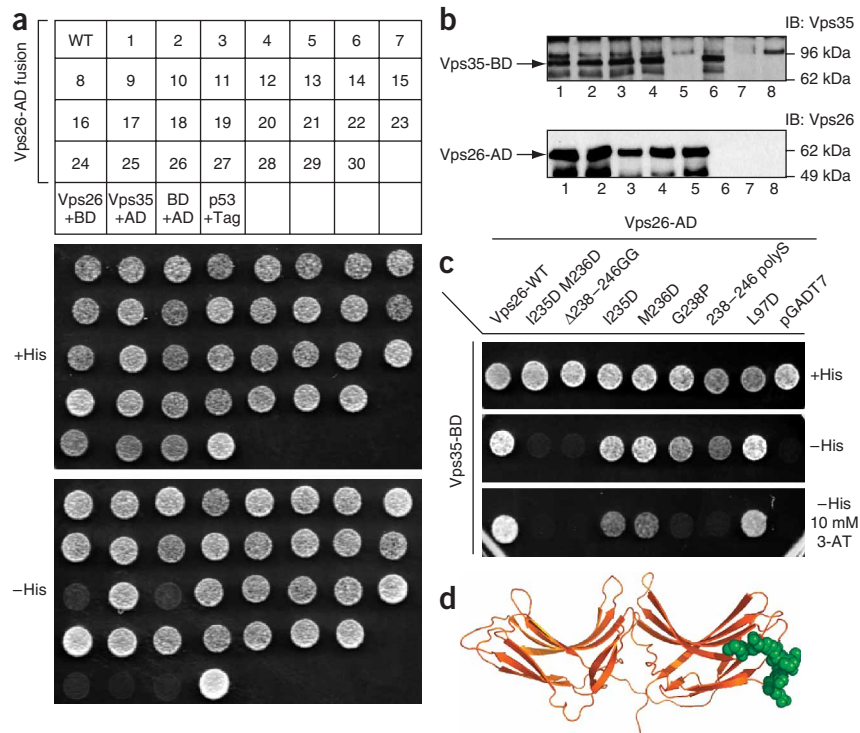
contains clusters of buried polar interactions (**Fig. 4a,b**). The overall extents of the polar cores are similar, although the identities of individual amino acids are not conserved (**Fig. 4c,d**).

Mapping the binding site for Vps35 on Vps26

Vps26 interacts directly with Vps35 (refs. 32,33). To identify the binding site for Vps35 on Vps26, we constructed 30 mutants of Vps26 carrying substitutions of surface residues (**Table 1** and **Fig. 5**, constructs 1–30). These mutations included nonconservative substitutions of single residues or clusters of 2–4 residues, and in one case the replacement of the loop comprising residues 238–246 by a Gly-Gly linker sequence. The design of this latter mutation enabled deletion of the loop while still allowing the linkage of the adjoining sequences

without conformational distortion of the protein. The choice of these mutation sites was based on several criteria: conservation, exposed hydrophobic residues, location in concave surface regions, correspondence to functional sites in arrestin and unusually strong positive or negative electrostatic potential, all of which are likely properties of interaction sites. The interaction of these Vps26 mutants with Vps35 was tested using a yeast two-hybrid system in which Vps26 variants and Vps35 were expressed as fusions with the transcription activation domain (Gal4AD) and DNA-binding domain (Gal4BD) of the Gal4 transcription factor, respectively. We observed that the mutation I235D M236D (construct 16) or deletion of the 238–246 loop (construct 18; Δ238–246 GG) abrogated interaction with Vps35, whereas the other 28 mutations had no detectable effect (**Fig. 5a**).

Figure 5 Identification of the Vps35-binding site on Vps26. **(a)** Interaction of Vps35 fused to Gal4BD with wild-type or mutant Vps26 constructs (numbered from 1 to 30 in **Table 1**) fused to Gal4AD was analyzed using the yeast two-hybrid system. Ability to grow in the absence of histidine (–His) is indicative of interactions. A summary of the results from three independent experiments is presented in **Table 1** and a representative experiment is shown in the figure. Negative and positive controls for interactions described in Methods are also shown. I235D M236D (construct 16) and Δ 238–246 GG (construct 18) Vps26 transformants do not grow on –His plates. BD, pGBKY7; AD, pGADT7. **(b)** Whole-cell extracts of cotransformed cells from the yeast two-hybrid assay, expressing Vps35 together with wild-type Vps26 (WT, lane 1), I235D M236D Vps26 (construct 16, lane 2), Δ 238–246 GG Vps26 (18, lane 3), L250D F251D Vps26 (12, lane 4), Vps35 and pGADT7 (lane 6), pGBKT7 and WT Vps26 (lane 5), pGBKT7 and pGADT7 (lane 7), or p53 and SV40 large T-antigen (Tag, lane 8), were subjected to SDS-PAGE and immunoblotting (IB) using polyclonal antibodies to Vps35 (top) and Vps26 (bottom). **(c)** Additional Vps26 mutants were tested for interaction with Vps26 using the yeast two-hybrid system. A summary of the results is presented in **Table 1** and a representative experiment is shown in the figure. 238–246 polyS and G238P mutants of Vps26 do not support growth on –His plates in the presence of the competitive inhibitor of the His3 protein, 3-AT. **(d)** Residues involved in binding Vps26 are highlighted in a space-filling model. Residues that are disordered in the Vps26 structure were modeled in a sterically allowed but otherwise arbitrary conformation.



Immunoblot analysis showed that the binding-defective mutants were expressed at levels similar to those of wild-type Vps26 and other Vps26 mutants (**Fig. 5b**). Notably, both of these mutations map to the same region of Vps26, the distal tip of the C domain (**Fig. 5d**). The 28 other single and multiple mutations tested represent coverage of a total of 69 surface residues, including all of the likely interaction sites. The lack of any effect on the Vps35 interaction rules out these regions as candidate binding sites. We conclude that Vps35 binds a single isolated site on Vps26 located at one tip of the molecule.

To map the determinants of Vps26 binding to Vps35 in more detail, several additional mutations in the loop region were generated (**Table 1** and **Fig. 5c**, constructs 31–34). The histidine biosynthesis inhibitor 3-aminotriazole (3-AT) was used in one set of assays to achieve higher stringency and resolve weaker mutational effects. The entire mobile loop was replaced by a polyserine linker in one construct, 238–246 polyS. This mutant construct showed interaction with Vps35 in the absence of 3-AT, but not in its presence (**Fig. 5c**). Similarly, substitution of loop residue Gly238 by proline resulted in detection of an interaction with Vps35 in the absence, but not the presence, of 3-AT (**Fig. 5c**). A construct consisting of only loop residues 232–247 did not interact with Vps35 in the two-hybrid assay (data not shown). We conclude that the mobile loop and adjacent residues are the primary binding site for Vps35. The loop is not autonomous, however, and it must be presented in the context of the Vps26 fold.

To determine whether the same mutations affected the assembly of Vps26 with Vps35 in human cells, we transfected HeLa cells with mammalian expression plasmids encoding myc-tagged wild-type or mutant Vps26 constructs (**Fig. 6**). These constructs were then isolated by immunoprecipitation with an antibody to the myc epitope and the

immunoprecipitates were analyzed by SDS-PAGE and immunoblotting with antibodies to Vps35 and Vps29. We found that, whereas the wild-type and R69A E71A Vps26 constructs coprecipitated endogenous Vps35 and Vps29, the I235D M236D, Δ 238–246 GG, 238–246 polyS and G238P Vps26 constructs did not (**Fig. 6a**). This was despite similar levels of expression of all recombinant myc-tagged constructs in the transfected cells (**Fig. 6a**). Therefore, mutations in the loop and adjacent regions not only prevent interaction of Vps26 with Vps35 but also block the incorporation of Vps26 into the endogenous Vps26–Vps29–Vps35 subcomplex. This is consistent with the notion that Vps26 interacts with retromer only in the context of the Vps26–Vps29–Vps35 subcomplex and defines the mechanism of Vps26 integration into the retromer.

We also examined the intracellular localization of the different myc-tagged Vps26 constructs by immunofluorescence microscopy. We observed that, whereas the wild-type and R69A E71A Vps26 constructs colocalized with endogenous SNX1 on endosomes, the I235D M236D, Δ 238–246 GG, 238–246 polyS and G238P Vps26 constructs showed a diffuse cytosolic distribution (**Fig. 6b**). These results agree with those of the coprecipitation experiments and provide further evidence that recruitment of Vps26 to endosomes requires its assembly with Vps29 and Vps35.

Next, we investigated the effect of Vps26 mutations on retromer function in *Saccharomyces cerevisiae*. Yeast Vps26 was tagged at its C terminus with green fluorescent protein (GFP), and mutants were constructed that were analogous to those previously made using human Vps26. The resulting Vps26–GFP constructs were expressed by transformation into a Vps26-null yeast strain (*vps26Δ*). The transformed strains were then examined for expression of the different Vps26 constructs and for processing and secretion of

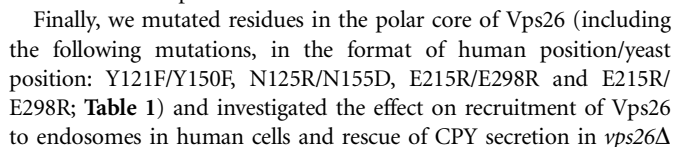


Figure 6 The binding site for Vps35 is required for Vps26 integration into the retromer complex *in vivo*. **(a)** Lysates from HeLa cells that were either not transfected (lanes 1 and 8, NT) or transfected with cDNAs encoding wild-type (WT) or indicated mutant forms of myc-tagged Vps26 were subjected to immunoprecipitation (IP) using a mouse monoclonal antibody to the myc epitope. Lysates (1% of total, lanes 1–7) and immunoprecipitates (lanes 8–14) were then analyzed by SDS-PAGE and immunoblotting with antibodies (Abs) to the myc epitope (top panel), Vps35 (middle panel) or Vps29 (bottom panel). **(b)** Intracellular localization of Vps26-myc and the Vps26-myc mutants indicated (left column shows Alexa 488 green channel), as well as colocalization of these constructs with SNX1 (middle column shows Alexa 546 red channel), was examined in fixed and permeabilized cells by indirect immunofluorescence and confocal microscopy. Right column shows merged images; yellow indicates colocalization.

The inactive conformations of v-arrestin^{31,35} and β -arrestin^{36,37} are locked in place by interactions between the interdomain linker, the



C-terminal loop and the polar core. The active conformation of arrestin has been inferred from mutational³⁸ and proteolytic³⁹ analyses. Upon receptor phosphorylation, a phospho-serine in the receptor tail binds Arg175 in the polar core. This destabilizes the polar core such that the two β -sandwich domains can reorient with respect to each other and embrace the GPCR through their concave surfaces⁴⁰. v-arrestin Arg175 is replaced by hydrophobic residues in Vps26 orthologs, suggesting that there is no arrestin-like phosphate sensor in the Vps26 family. We have mutated four polar-core residues in Vps26, and these mutations do not interfere with endosomal localization in human cells or CPY sorting in yeast, so the functional significance of the polar core in Vps26 is currently unclear.

The second major observation in this study is that Vps26 binds Vps35 and is integrated into the retromer complex via an exposed surface loop near the tip of the C-terminal domain. As the Vps35-binding site involves only the tip of one domain, Vps35 interactions should be independent of any rearrangements of the two Vps26 domains relative to each other. This would allow Vps26 to undergo a regulatory conformational cycle while remaining integrated in the complex. The importance of this loop is highlighted by its conservation in Vps26 orthologs and paralogs. A second Vps26 isoform, Vps26B, has recently been described²⁷ and is reported to localize to the plasma membrane, rather than to endosomes. As the surface loop contains the determinants for the endosomal localization of Vps26A, it will be interesting to understand the mechanism for the apparently distinct localization of Vps26B. This loop is also conserved in yeast Vps26. We have found a marked correlation between loss of human Vps35 binding and endosomal localization in tissue-culture cells and loss of the CPY-sorting function in yeast.

The determinants for Vps35 binding include two hydrophobic residues and a glycine residue. The key role of a glycine suggests that the loop binds a well-defined pocket on the surface of Vps35 that requires an unusual conformation of the loop, is sterically tightly packed or both. One precedent for such a role for a glycine residue is provided by the GGA appendage-binding motifs of rabaptin-5 and related proteins^{41,42}. The key functional role of the two hydrophobic residues suggests a hydrophobic character for at least part of the pocket on Vps35.

Vps26 has been the most mysterious of the five retromer subunits because of the absence of recognizable homology to any other protein of known structure or function and the lack of identified interactions with other proteins. The findings in this study now provide a structural foothold for understanding the function of Vps26 orthologs. We now know that Vps26 shares a common architecture with the arrestins. The similarities are extensive enough to suggest that Vps26 undergoes an arrestin-like conformational change that enables it to bind transmembrane receptors of some kind. It will be important to test this idea and to seek the identity of the putative receptors that interact with Vps26 orthologs and the factors that control the putative conformational change. Although these concepts of receptor binding and conformational change remain to be tested, the observations in this study provide compelling evidence for a mechanism by which Vps26 orthologs are assembled into the retromer. We have found that the Vps35-binding site on Vps26 is essential for localization in mammalian cells and for function in yeast, and it seems likely that these findings will be general across other species.

METHODS

Protein expression, purification and crystallization. PCR was used to amplify the complementary DNA coding for human Vps26A and to add a C-terminal

His₅ tag (GLVPRGSHHHH). The product was inserted into the pmr101A (modified pmr101; American Type Culture Collection) vector using the NdeI and XhoI restriction sites. The expressed recombinant protein contains the additional dipeptide Met-Gly at the N terminus as a result of the vector construction. Protein was expressed in the BL21 (DE3) star (Invitrogen) strain at 20 °C overnight. Vps26 was purified on a 5-ml HiTrap chelating HP column (GE Healthcare) and eluted with a gradient of 12.5–300 mM imidazole in a buffer containing 20 mM Tris (pH 8.0), 50 mM NaCl and 5% (v/v) glycerol. The eluted fractions were pooled, diluted by adding an equal volume of water and purified by ion exchange (5-ml HiTrap Q FF) and gel filtration (Superdex 75 16/60) (GE Healthcare). Fractions were pooled and concentrated to 8 mg ml⁻¹ in 10 mM Tris (pH 8.0), 5% (v/v) glycerol, 100 mM NaCl and 10 mM DTT for crystallization.

Diffraction-quality crystals used for native data collection were obtained using buffer containing 100 mM sodium cacodylate (pH 6.5), 15% (v/v) glycerol, 8% (w/v) PEG 10,000, 10 mM DTT and 1 mM TmCl₃ by microseeding. SeMet-substituted protein was produced using the same strain growing in media containing 1 g NH₄Cl, 3 g KH₂PO₄, 6 g Na₂HPO₄•7H₂O, 2.5 g NaAc•3H₂O, 1.5 g succinic acid, 20 g glucose, 500 mg MgSO₄•7H₂O, 13.9 mg FeSO₄•7H₂O and 10 ml Kao and Michayluk vitamin solution (100×) (Sigma) per liter, and the pH was adjusted to 7.4 with NaOH. D,L-SeMet was added to the media when the cells had grown to A₆₀₀ = 0.5, to a final concentration of 100 µg ml⁻¹. The culture was induced 20 min after the addition of SeMet and harvested after overnight incubation at 20 °C. The expression, purification and crystallization of the selenium-derivative protein were carried out under the same conditions as that of native protein, except that GdCl₃ was used as a crystallization additive instead of TmCl₃. A platinum derivative was prepared by soaking native crystals in buffer containing 100 mM sodium cacodylate (pH 6.5), 20% (v/v) glycerol, 8% (w/v) PEG 10,000 and 10 mM Pt(NH₃)₂Cl₂ at 23 °C for 5 d.

Data collection and structure determination. Data were collected at 98 K at beamline ID-22, Advanced Photon Source (APS, Argonne National Lab; Table 2) and processed with HKL2000 (HKL Research). The structure was determined by combining a two-wavelength MAD data set from a SeMet crystal, a three-wavelength MAD data set from a platinum crystal and a single isomorphous replacement (SIR) analysis using the platinum crystal as a derivative. Six ordered selenium sites and one platinum site were identified using SOLVE⁴³. Subsequent phasing and solvent flattening was carried out using SOLVE⁴³ and RESOLVE⁴⁴. The solved structure revealed electron density attached to the two cysteine residues of Vps26; we attribute this to covalently bound dimethylarsenate, which was included in the refined model. Iterative cycles of model building and refinement were carried out using the O⁴⁵, CNS⁴⁶ and CCP4⁴⁷ program packages. A portion (8.8%) of the data was used for cross-validation in CNS.

Recombinant DNA constructs. An EcoRI-XhoI fragment encoding human Vps26A (residues 2–327) obtained from the Vps26A-pB42AD construct³² was subcloned into the corresponding sites of the pGADT7 vector (Clontech) and the pcDNA3.1/myc-His vector (Invitrogen). Addition of a start codon (position 1) and removal of a stop codon (position 327) from the Vps26A-pcDNA3.1 construct was done by site-directed mutagenesis. An MfeI-BamHI fragment encoding Vps35 (residues 2–796) was obtained from the Vps35-pLexA construct³² and later subcloned into the EcoRI and BamHI sites of the pGBKT7 vector (Clontech). An EcoRI-BamHI fragment encoding full-length *S. cerevisiae* Vps26p was cloned into the pRS316 (C-terminal GFP) vector. Mutagenesis of the Vps26A-pGADT7, Vps26A-myc-pcDNA3.1 and Vps26p-pRS316 constructs was performed using the QuikChange site-directed mutagenesis kit (Stratagene). All the constructs were sequenced to confirm their identities and the presence of the desired mutations.

Yeast two-hybrid assay. The *S. cerevisiae* strain AH-109 (Clontech) was transformed by the lithium acetate procedure. Yeast cells were cotransformed with cDNAs encoding wild-type Vps35 fused to Gal4BD (Vps35-pGBKT7) and wild-type or mutant Vps26A fused to GAL4AD (Vps26-pGADT7). After selection, the cotransformants were spotted on plates containing or lacking histidine. As negative controls, the AH-109 strain was cotransformed with

Table 2 Data collection, phasing and refinement statistics

	Native	Selenium			Platinum	
Data collection						
Space group	$P2_12_12_1$	$P2_12_12_1$			$P2_12_12_1$	
Cell dimensions						
<i>a</i> , <i>b</i> , <i>c</i> (Å)	41.0, 76.7, 126.5	41.14, 77.06, 126.8			40.6, 76.2, 128.4	
		<i>Inflection</i>	<i>Remote</i>	<i>Peak</i>	<i>Inflection</i>	<i>Remote</i>
Wavelength (Å)	1.072	0.9794	0.9686	1.072	1.054	1.5418
Resolution (Å)	2.1	3.0	3.0	2.5	2.7	2.6
<i>R</i> _{merge}	4.3 (34.7)	7.5 (14.1)	7.6 (10.1)	8.1 (21.9)	6.9 (22.8)	6.9 (50.4)
<i>I</i> / σ <i>I</i>	21.3	16.0	13.8	13.4	14	18.3
Completeness (%)	92.2 (81.8)	96.5 (89.1)	97.4 (75.6)	98.5 (96.1)	98.9 (97.0)	98.1 (87.5)
Redundancy	7	10	11	8	4	13
Refinement						
Resolution (Å)	2.1					
No. reflections	21,275					
<i>R</i> _{work} / <i>R</i> _{free}	23.4/28.5					
No. atoms						
Protein	2,380					
Ligand/ion	6					
Water	89					
<i>B</i> -factors						
Protein	65.765					
Ligand/ion	75.9					
Water	63.85					
R.m.s deviations						
Bond lengths (Å)	0.008					
Bond angles (°)	1.37					

Three crystals were used for structure solving and refinement. Highest-resolution shell is shown in parentheses.

Vps26-pGADT7 and pGBKT7, Vps35-pGBKT7 and pGADT7, and the 'empty' vectors pGBKT7 and pGADT7. As a positive control for growth on histidine-lacking plates, cells were cotransformed with p53-pGBKT7 and SV40-LT-Ag-pGADT7 (Tag). AH-109 transformants were grown overnight at 30 °C in media lacking leucine and tryptophan. The day of the experiment, the yeast cell cultures were diluted to $A_{600} = 0.4$ and grown for 2 h at 30 °C. The cells were then harvested at 1,000g, washed and resuspended in medium lacking leucine and tryptophan to 0.1 A_{600} ml⁻¹. Five μ l of each suspension was spotted on plates lacking leucine and tryptophan, in the presence or absence of histidine, and incubated at 30 °C for 2–3 d. Whole-cell lysates of the transformants were obtained according to published protocols⁴⁸ and subjected to SDS-PAGE and immunoblot analysis.

Immunoprecipitation. HeLa cells (American Type Culture Collection) were cultured on 100-mm dishes as described previously⁴⁹. When the cells reached 80%–90% confluency, they were transfected with 24 μ g of pcDNA3.1 encoding myc-tagged forms of wild-type, I235D M236D, Δ 238–246 GG, 238–246 polyS, G238P or R69A E71A Vps26, using Lipofectamine 2000 (Invitrogen). At 24 h after transfection, cells were washed twice with ice-cold PBS and immediately resuspended in 1 ml lysis buffer (0.5% (v/v) Triton X-100, 300 mM NaCl, 50 mM Tris-HCl (pH 7.4), 5 mM EDTA) supplemented with a protease inhibitor cocktail (Roche). After 30 min of incubation at 4 °C, lysates were centrifuged at 16,000g for 15 min. The supernatants were then precleared by incubation for 60 min at 4 °C with 30 μ l protein G-Sepharose beads (Amersham Pharmacia Biotech) and centrifugation at 8,000g for 5 min. The precleared lysates were incubated for 2 h at 4 °C with 30 μ l protein G-Sepharose beads bound to mouse monoclonal antibody to myc (9E10; Covance). After immunoprecipitation, the beads were washed four times with ice-cold wash buffer (0.1% (w/v) Triton X-100, 300 mM NaCl, 50 mM Tris-HCl (pH 7.4)) and once with ice-cold PBS. Washed beads were then subjected to SDS-PAGE and immunoblotting analysis. Antibodies to Vps29 and Vps35 have been described³².

Immunofluorescent labeling and scanning-laser confocal microscopy. HeLa cells grown on glass cover slips and transfected with wild-type and mutant Vps26A-myc-pcDNA3.1 constructs were washed with PBS and fixed for 10 min with 4% (w/v) paraformaldehyde in PBS at room temperature. Cells were rinsed twice with PBS, and excess paraformaldehyde was quenched with PBS containing 20 mM glycine (pH 8.0) and 75 mM NH₄Cl for 15 min at room temperature. The cells were again washed with PBS and permeabilized with 0.025% (w/v) saponin prepared in blocking solution (PBS containing 5% (v/v) goat serum and 7 mg ml⁻¹ fish skin gelatin) for 10 min at 37 °C in a humidified chamber. Cells were immunostained with mouse monoclonal antibody to myc (9E10) and polyclonal antibody to SNX1 for 2 h at 37 °C, then incubated with fluorescently labeled secondary antibodies. Imaging was performed on a TCS SP-2 confocal microscope (Leica) equipped with argon-krypton and 543/594-nm helium-neon lasers. Images were acquired using a \times 63 Plan-Apochromat oil objective (NA 1.4) and the appropriate filter combination. Settings were as follows: photomultipliers set to 500–700 V, Airy = 1, zoom = 3.0–4.0, Kalman filter ($n = 8$). The images (512 \times 512 pixels) were saved in a tag information file format (TIFF), contrast was corrected in Adobe Photoshop and images were imported into Macromedia Freehand MX.

Yeast growth and CPY-sorting assays. The Vps26 Δ :KanMX deletion *S. cerevisiae* strain was obtained from Research Genetics (Invitrogen), and its ability to sort and process CPY was compared with the parental strain BY4742 (data not shown). Yeast cells were maintained on YPD plates or grown in liquid medium before transformation with yeast expression plasmids. Transformation with pRS316 encoding GFP-tagged forms of wild-type, I318D M319D, Δ 321–328 GG, 321–328 polyS or G321P Vps26, or encoding GFP, into the vps26 Δ strain was performed by the lithium acetate procedure.

Cells transformed with wild-type and mutant Vps26p-GFP-pRS316 were metabolically labeled with the ³⁵S Express reagent (Perkin Elmer Life Sciences) for 10 min (pulse) and chased for 30 min as previously described⁴⁸.

Immunoprecipitations using mouse anti-CPY (Molecular Probes) conjugated to protein G-Sepharose beads were performed overnight at 4 °C as previously described⁴⁸ and the immunoprecipitates were analyzed by SDS-PAGE and autoradiography. Dried gels were also scanned on a PhosphorImager (Typhoon 9200, Molecular Dynamics).

The CPY colony blot assay was adapted from ref. 50. Yeast transformants grown in selection medium ($A_{600} = 10^{-3}$) were spotted onto a YPD plate and overlaid with a nitrocellulose membrane. The plates were incubated for 22–24 h at 30 °C. The nitrocellulose membranes were washed with water and immunoblotted with mouse anti-CPY and the appropriate horseradish peroxidase-conjugated secondary antibody. Visualization was done with enhanced chemiluminescence reagents (Perkin Elmer Life Sciences).

Accession codes. Protein Data Bank: Coordinates have been deposited with accession code 2FAU.

Note: Supplementary information is available on the Nature Structural & Molecular Biology website.

ACKNOWLEDGMENTS

We thank B. Beach and X. Zhu for technical assistance, W. Smith for liposome binding studies, H. Watson and C. Bonangelino for advice on CPY-sorting assays, C. Haft for reagents and comments on the manuscript and D. Hurt, G. Miller and the staff of beamline 22-ID, APS, Argonne National Laboratory for assistance with X-ray data collection. This research was supported by the US National Institutes of Health through the intramural programs of the National Institute of Diabetes and Digestive and Kidney Diseases (to J.H.H.) and the National Institute of Child Health and Human Development (to J.S.B.). Use of the APS was supported by the US Department of Energy, Basic Energy Sciences, Office of Science, under contract no.W-31-109-Eng-38.

COMPETING INTERESTS STATEMENT

The authors declare that they have no competing financial interests.

Published online at <http://www.nature.com/nsmb/>

Reprints and permissions information is available online at <http://npg.nature.com/reprintsandpermissions/>

- Ghosh, P., Dahms, N.M. & Kornfeld, S. Mannose 6-phosphate receptors: new twists in the tale. *Nat. Rev. Mol. Cell Biol.* **4**, 202–212 (2003).
- Bonifacino, J.S. The GGA proteins: adaptors on the move. *Nat. Rev. Mol. Cell Biol.* **5**, 23–32 (2004).
- Meyer, C. *et al.* mu1A-adaptin-deficient mice: lethality, loss of AP-1 binding and rerouting of mannose 6-phosphate receptors. *EMBO J.* **19**, 2193–2203 (2000).
- Doray, B., Ghosh, P., Griffith, J., Geuze, H.J. & Kornfeld, S. Cooperation of GGAs and AP-1 in packaging MPRs at the trans-Golgi network. *Science* **297**, 1700–1703 (2002).
- Diaz, E. & Pfeffer, S.R. TIP47: A cargo selection device for mannose 6-phosphate receptor trafficking. *Cell* **93**, 433–443 (1998).
- Wan, L. *et al.* PACS-1 defines a novel gene family of cytosolic sorting proteins required for trans-Golgi network localization. *Cell* **94**, 205–216 (1998).
- Bowers, K. & Stevens, T.H. Protein transport from the late Golgi to the vacuole in the yeast *Saccharomyces cerevisiae*. *Biochim. Biophys. Acta* **1744**, 438–454 (2005).
- Seaman, M.N. Recycle your receptors with retromer. *Trends Cell Biol.* **15**, 68–75 (2005).
- Horazdovsky, B.F. *et al.* A sorting nexin-1 homologue, vps5p, forms a complex with vps17p and is required for recycling the vacuolar protein-sorting receptor. *Mol. Biol. Cell* **8**, 1529–1541 (1997).
- Seaman, M.N.J., McCaffery, J.M. & Emr, S.D. A membrane coat complex essential for endosome-to-Golgi retrograde transport in yeast. *J. Cell Biol.* **142**, 665–681 (1998).
- Seaman, M.N.J. & Williams, H.P. Identification of the functional domains of yeast sorting nexins Vps5p and Vps17p. *Mol. Biol. Cell* **13**, 2826–2840 (2002).
- Cheever, M.L. *et al.* Phox domain interaction with PtdIns(S)P targets the Vam7 t-SNARE to vacuole membranes. *Nat. Cell Biol.* **3**, 613–618 (2001).
- Kanai, F. *et al.* The PX domains of p47phox and p40phox bind to lipid products of PI(3)K. *Nat. Cell Biol.* **3**, 675–678 (2001).
- Xu, Y., Hortsman, H., Seet, L., Wong, S.H. & Hong, W. SNX3 regulates endosomal function through its PX-domain-mediated interaction with PtdIns(3)P. *Nat. Cell Biol.* **3**, 658–666 (2001).
- Elison, C.D. *et al.* PtdIns(3)P regulates the neutrophil oxidase complex by binding to the PX domain of p40(phox). *Nat. Cell Biol.* **3**, 679–682 (2001).
- Virbasius, J.V. *et al.* Activation of the Akt-related cytokine-independent survival kinase requires interaction of its phox domain with endosomal phosphatidylinositol 3-phosphate. *Proc. Natl. Acad. Sci. USA* **98**, 12908–12913 (2001).
- Peter, B.J. *et al.* BAR domains as sensors of membrane curvature: The amphiphysin BAR structure. *Science* **303**, 495–499 (2004).
- Nothwehr, S.F., Bruinsma, P. & Strawn, L.A. Distinct domains within Vps35p mediate the retrieval of two different cargo proteins from the yeast prevacuolar/endosomal compartment. *Mol. Biol. Cell* **10**, 875–890 (1999).
- Arighi, C.N., Hartnell, L.M., Aguilar, R.C., Haft, C.R. & Bonifacino, J.S. Role of the mammalian retromer in sorting of the cation-independent mannose 6-phosphate receptor. *J. Cell Biol.* **165**, 123–133 (2004).
- Carlton, J. *et al.* Sorting nexin-1 mediates tubular endosome-to-TGN transport through coincidence sensing of high-curvature membranes and 3-phosphoinositides. *Curr. Biol.* **14**, 1791–1800 (2004).
- Seaman, M.N. Cargo-selective endosomal sorting for retrieval to the Golgi requires retromer. *J. Cell Biol.* **165**, 111–122 (2004).
- Zhong, Q. *et al.* Determinants of the endosomal localization of sorting nexin 1. *Mol. Biol. Cell* **16**, 2049–2057 (2005).
- Wang, D. *et al.* Crystal structure of human vacuolar protein sorting protein 29 reveals a phosphodiesterase/nuclease-like fold and two protein-protein interaction sites. *J. Biol. Chem.* **280**, 22962–22967 (2005).
- Collins, B.M., Skinner, C.F., Watson, P.J., Seaman, M.N. & Owen, D.J. Vps29 has a phosphoesterase fold that acts as a protein interaction scaffold for retromer assembly. *Nat. Struct. Biol.* **12**, 594–602 (2005).
- Lee, J.J., Radice, G., Perkins, C.P. & Costantini, F. Identification and characterization of a novel, evolutionarily conserved gene disrupted by the murine Hb58 embryonic lethal insertion. *Development* **115**, 227–288 (1992).
- Small, S.A. *et al.* Model-guided microarray implicates the retromer complex in Alzheimer's disease. *Ann. Neurol.* **58**, 909–919 (2005).
- Kerr, M.C. *et al.* A novel mammalian retromer component, Vps26B. *Traffic* **6**, 991–1001 (2005).
- Lefkowitz, R.J. & Whalen, E.J. beta-arrestins: traffic cops of cell signaling. *Curr. Opin. Cell Biol.* **16**, 162–168 (2004).
- Hurley, J.H. & Misra, S. Signaling and subcellular targeting by membrane-binding domains. *Annu. Rev. Biophys. Biomol. Struct.* **29**, 49–79 (2000).
- Holm, L. & Sander, C. Dali—a network tool for protein-structure comparison. *Trends Biochem. Sci.* **20**, 478–480 (1995).
- Hirsch, J.A., Schubert, C., Gurevich, V.V. & Sigler, P.B. The 2.8 angstrom crystal structure of visual arrestin: a model for arrestin's regulation. *Cell* **97**, 257–269 (1999).
- Haft, C.R. *et al.* Human orthologs of yeast vacuolar protein sorting proteins Vps26, 29, and 35: assembly into multimeric complexes. *Mol. Biol. Cell* **11**, 4105–4116 (2000).
- Reddy, J.V. & Seaman, M.N. Vps26p, a component of retromer, directs the interactions of Vps35p in endosome-to-Golgi retrieval. *Mol. Biol. Cell* **12**, 3242–3256 (2001).
- Goodman, O.B. *et al.* beta-arrestin acts as a clathrin adaptor in endocytosis of the beta(2)-adrenergic receptor. *Nature* **383**, 447–450 (1996).
- Granzin, J. *et al.* X-ray crystal structure of arrestin from bovine rod outer segments. *Nature* **391**, 918–921 (1998).
- Han, M., Gurevich, V.V., Vishnivetskiy, S.A., Sigler, P.B. & Schubert, C. Crystal structure of beta-arrestin at 1.9 angstrom: Possible mechanism of receptor binding and membrane translocation. *Structure* **9**, 869–880 (2001).
- Milano, S.K., Pace, H.C., Kim, Y.M., Brenner, C. & Benovic, J.L. Scaffolding functions of arrestin-2 revealed by crystal structure and mutagenesis. *Biochemistry* **41**, 3321–3328 (2002).
- Vishnivetskiy, S.A., Hirsch, J.A., Velez, M.G., Gurevich, Y.V. & Gurevich, V.V. Transition of arrestin into the active receptor-binding state requires an extended interdomain hinge. *J. Biol. Chem.* **277**, 43961–43967 (2002).
- Xiao, K.H., Shenoy, S.K., Nobles, K. & Lefkowitz, R.J. Activation-dependent conformational changes in beta-arrestin 2. *J. Biol. Chem.* **279**, 55744–55753 (2004).
- Vishnivetskiy, S.A., Hosey, M.M., Benovic, J.L. & Gurevich, V.V. Mapping the arrestin-receptor interface—structural elements responsible for receptor specificity of arrestin proteins. *J. Biol. Chem.* **279**, 1262–1268 (2004).
- Miller, G.J., Mattern, R., Bonifacino, J.S. & Hurley, J.H. Recognition of accessory protein motifs by the gamma-adaptin ear domain of GGA3. *Nat. Struct. Biol.* **10**, 599–606 (2003).
- Collins, B.M., Praefcke, G.J.K., Robinson, M.S. & Owen, D.J. Structural basis for binding of accessory proteins by the appendage domain of GGAs. *Nat. Struct. Biol.* **10**, 607–613 (2003).
- Terwilliger, T.C. & Berendzen, J. Automated MAD and MIR structure solution. *Acta Crystallogr. D Biol. Crystallogr.* **55**, 849–861 (1999).
- Terwilliger, T.C. Maximum-likelihood density modification. *Acta Crystallogr. D Biol. Crystallogr.* **56**, 965–972 (2000).
- Jones, T.A., Zou, J.Y., Cowan, S.W. & Kjeldgaard, M. Improved methods for building protein models in electron-density maps and the location of errors in these models. *Acta Crystallogr. A* **47**, 110–119 (1991).
- Brunger, A.T. *et al.* Crystallography & NMR system: a new software suite for macromolecular structure determination. *Acta Crystallogr. D Biol. Crystallogr.* **54**, 905–921 (1998).
- Collaborative Computational Project, Number 4. The CCP4 suite: programs for protein crystallography. *Acta Crystallogr. D Biol. Crystallogr.* **50**, 760–763 (1994).
- Bonifacino, J.S. & Dell'Angelica, E.C. Protein labeling and immunoprecipitation. in *Current Protocols in Cell Biology* (eds. Bonifacino, J.S., Dasso, M., Harford, J.B., Lippincott-Schwartz, J. & Yamada, K.M.) 7.0.0–7.2.10 (John Wiley and Sons, New York, 1998).
- Mattern, R., Arighi, C.N., Lodge, R., Zerial, M. & Bonifacino, J.S. Divalent interaction of the GGAs with the Rabaptin-5-Rabex-5 complex. *EMBO J.* **22**, 78–88 (2003).
- Bonangelino, C.J., Chavez, E.M. & Bonifacino, J.S. Genomic screen for vacuolar protein sorting genes in *Saccharomyces cerevisiae*. *Mol. Biol. Cell* **13**, 2486–2501 (2002).